Supplemental Material: Charge Condensation and Lattice Coupling Drives Stripe Formation in Nickelates

This document provides additional details of the X-ray measurements, sample preparation and the wavevectors of charge order (CO) and spin order (SO) peaks.

X-RAY MEASUREMENTS

All X-ray measurements were carried out at the Coherent Soft X-Ray (CSX) 23-ID-1 beamline at the National Synchrotron Light Source II (NSLS-II) that is dedicated to resonant coherent soft x-ray studies. NSLS-II was used in its standard mode with 1320 electron buckets and 2 ps between the buckets [1]. CSX at NSLS-II has rather ideal properties for these experiments as it delivers an extremely high coherent flux of $\sim 10^{13}$ photons/s at the sample. This is, at the time of writing, state-of-the-art in time-averaged coherent flux even including current x-ray free electron lasers, which, despite their very high peak flux, have similar or lower time-averaged flux.

To enhance the signals from CO and SO, we tuned the incident energy to find the Ni L_3-edge resonance for both orders separately, as these occur at slightly different energies [2]. Figure S1 shows the resonant profile of the CO and SO. These results are consistent with prior resonant x-ray scattering on $La_{2-x}Sr_xNiO_4$ [2]. An overview of resonant soft x-ray scattering is available in Ref. [3]. The X-ray polarization was also chosen, using the CSX elliptically polarized undulator, to maximize the signal. As has been proven previously, SO is optimized via π X-ray polarization and CO is similarly strong with either σ or π polarization [2]. Data were collected using a fast CCD with 30×30 μm^2 pixel size that is 340 mm from the sample. This gives a reciprocal space resolution of 3.8×10^{-5} $Å^{-1}$/pixel.

In standard X-ray photon correlation spectroscopy (XPCS), the time resolution is determined by how frequently the detector is read out. This is chosen considering (a) the speed of the dynamics (b) read-out noise from the detector, (c) the minimal time required to achieve sufficient signal, and (d) the maximum read-out rate of the detector (in our case every 10 ms). As described in the main text, we can exclude any significant fluctuations faster than about 10 s, since fast dynamics would reduce the speckle contrast via averaging over the measured time frame [4]. We chose the CCD read out time for the measurements based mainly on considerations (a)-(c). The CCD was read out every 1 s at 70 K. In this regime we detect of order 100 photons per pixel and 1 million photons/frame and cover well over $> 90\%$ of the total CO and SO Bragg peak intensity. We therefore have high confidence that the signals represent the domain dynamics on length scales down to ~ 100 nm, which is the characteristic lengthscale of the smallest CO and SO domains we measure. At temperatures with weaker scattering the read-out time was increased to up to 5 s.

After any temperature change, the experiment, and in particular the cryostat, was left to equilibrate for a minimum of 30 minutes following previously established procedures to stabilize the setup [4–6].

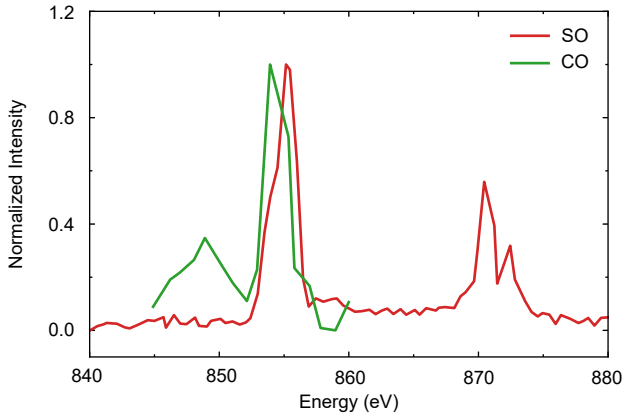

FIG. S1. Intensities of the superlattice peaks of CO and SO as a function of phonon energy.

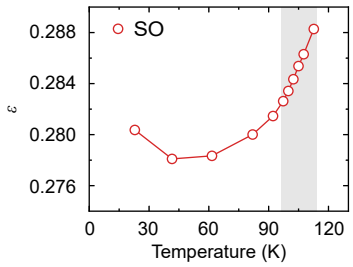

FIG. S2. Incommensurability derived from the SO $\boldsymbol{Q}$ vector as a function of temperature. The shaded areas indicate the onset temperature range for CO and SO.

SAMPLE PREPARATION

To realize a clean surface for the measurement, we polished the sample in water with sequence of P250 (sandpaper), P600 (sandpaper), 1 micron and 0.25 microns diamond. All steps were performed for about 1 min except for the last one which lasted 2 to 3 min.

In the measurement of domain memory, the sample position could drift during the sample cooling and warming process. To make sure that the same sample volume was illuminated in spite of the possible drift, we deposited a mask on the sample. This was done using a Field Electron and Ion (FEI) Helios 600 dual-beam focused-ion-beam (FIB) at the Center for Functional Nanomaterials (CFN). We deposited four 12 μm by 7 μm Pt pads with a thickness of 500 nm to form a square pinhole of approximately 5 μm by 5 μm in size inside a mask of about 19 μm by 19 μm. The x-ray beam was passed through a 10 μm conventional pinhole approximately 5 mm upstream of the sample to form a beam of about 11 μm in diameter at the sample, overfilling the pinhole, but not the mask. As the Pt deposition was performed in high-vacuum, possible oxidation to the surface of the sample was avoided. Since the penetration depth of Pt at the Ni L_3-resonance is 72 nm, the Pt layer blocks x-ray very efficiently. After the temperature cycle, the sample position was scanned to re-align the beam to the center of the pinhole. The mask was not used during the measurements of the temporal stability of the speckle patterns since the beamline and sample were sufficiently stable in these circumstances and we benefited from using the full intensity of the beam.

CHARGE AND SPIN ORDER WAVEVECTORS

The stripes in $La_{2-x}Sr_xNiO_{4+\delta}$ (LSNO) run diagonally to the Ni-O bonds. We prepared the single crystal with a surface normal close to the $[H, H, 0]$ direction in order to access a (H, H, L) scattering plane. This plane contains the CO and SO peaks at wavevectors of $\boldsymbol{Q}_{\rm CO} = (N \pm \epsilon, N \pm \epsilon, L)$ with L being odd and $\boldsymbol{Q}_{\rm SO} = (N + 1/2 \pm \epsilon/2, N + 1/2 \pm \epsilon/2, L)$ with L being even or odd, where N is an integer, ϵ is the incommensurability parameter. In this way, $\boldsymbol{Q}_{\rm SO}$ occurs at detector angle of $2\theta = 155°$ and an approximate sample angle $\theta = 77°$, where $\theta = 0°$ puts the beam parallel to the sample surface. $\boldsymbol{Q}_{\rm CO}$ then occurs at $2\theta = 135°$ $\theta = 29°$. The SO reflections with odd L arise from hypothetical body-centered-stacked stripes. Peaks with even L are forbidden in the hypothetical body-centered-picture and can be thought of arising from stacking faults [7, 8]. The even L peaks get enhanced in samples with hole concentrations away from the commensurate value, 1/3, due to increasing stacking faults [9].

However, the domain motions corresponding to $L = 0$ versus $L = 1$ are expected to be rather similar. Considering the motion of a $(0.36, 0.36)$ 2D spin modulation within a single NiO layer. There are two such NiO layers per unit cell and each layer is (by the crystal symmetry) equally well coupled with its neighboring layers in the same cell and in another cell. The only class of defect motion within a layer that would appear in the ideal (0.36, 0.36, 1) reflection but not in the (0.36, 0.36, 0) reflection is when a motion in one layer is canceled by an opposite motion in the other direction in the other layers. This type of coordinated motion is not physically plausible, as sliding the density waves against each other would cost far more energy than sliding in the same direction. It is also worth emphasizing that stripe order in nickelates is a bulk phenomenon so that the motion of a perfectly ordered domain will involve displacing the domain wall and the nearby domains. In addition, we note that the $(1/2 - \epsilon/2, 1/2 - \epsilon/2, 1)$ reflection cannot be reached with Ni L-edge resonance as the required $\boldsymbol{Q}$ is larger than twice the momentum carried by the x-ray photons.

For completeness we plot the incommensurability, ϵ, derived from the SO in Fig. S2, which is slightly larger than that from CO. The small difference in incommensurability may come from finite precision in determining the sample

UB matrix and is comparable to our estimated uncertainty in alignment, noting that large angular motions and changing the x-ray energy and harmonics of the beamline undulator were required for the two measurements. We also present in Fig. S3 the speckle patterns after different delay times at different temperatures for CO and SO.

CALCULATIONS OF CROSS-CORRELATION FUNCTION

The cross-correlation function is used to quantitatively evaluate the speckle position changes. To so do, we first isolated the pure speckle patterns, which was done by dividing the raw image by the peak envelope that was estimated by fitting. Then the cross-correlation function is calculated through a pixel-to-pixel intensity correlation approach [5]:

$$A_{m,n} * B_{m,n} = \sum_{m'=-M}^{M} \sum_{n'=-N}^{N} A_{m',n'} B_{m+m',n+n'}. \tag{1}$$

where speckle patterns before and after temperature cycling are represented as two $M \times N$ matrices $A_{m,n}$ and $B_{m,n}$, respectively. Here, we chose an area of approximately 50×50 pixels as the input. The resulting cross-correlation matrix shows a peak at the center, the amplitude of which, $I(A, B)$, represents the similarity of these two images. Similarly, the auto-correlations can be obtained as $I(A, A)$ and $I(B, B)$. The normalized cross-correlation is then derived through:

$$\xi_{\mathrm{CC}} = \frac{I(A, B)}{\sqrt{I(A, A) \times I(B, B)}} \tag{2}$$

[1] "National Syncrotron light Source II Website," `https://www.bnl.gov/ps/accelerator/`, accessed: 2020-12-02.

[2] C. Schüßler-Langeheine, J. Schlappa, A. Tanaka, Z. Hu, C. F. Chang, E. Schierle, M. Benomar, H. Ott, E. Weschke, G. Kaindl, O. Friedt, G. A. Sawatzky, H. J. Lin, C. T. Chen, M. Braden, and L. H. Tjeng, "Spectroscopy of stripe order in $La_{1.8}Sr_{0.2}NiO_4$ using resonant soft x-ray diffraction," Physical Review Letters **95**, 156402 (2005).

[3] Jörg Fink, E Schierle, E Weschke, and J Geck, "Resonant elastic soft x-ray scattering," Reports on Progress in Physics **76**, 056502 (2013).

[4] X. M. Chen, V. Thampy, C. Mazzoli, A. M. Barbour, H. Miao, G. D. Gu, Y. Cao, J. M. Tranquada, M. P. M. Dean, and S. B. Wilkins, "Remarkable stability of charge density wave order in $La_{1.875}Ba_{0.125}CuO_4$," Physical Review Letters **117**, 167001 (2016).

[5] X. M. Chen, C. Mazzoli, Y. Cao, V. Thampy, A. M. Barbour, W. Hu, M. Lu, T. A. Assefa, H. Miao, G. Fabbris, G. D. Gu, J. M. Tranquada, M. P. M. Dean, S. B. Wilkins, and I. K. Robinson, "Charge density wave memory in a cuprate superconductor," Nature Communications **10**, 1435 (2019).

[6] Roopali Kukreja, Nelson Hua, Joshua Ruby, Andi Barbour, Wen Hu, Claudio Mazzoli, Stuart Wilkins, Eric E. Fullerton, and Oleg G. Shpyrko, "Orbital domain dynamics in magnetite below the Verwey transition," Phys. Rev. Lett. **121**, 177601 (2018).

[7] S. H. Lee and S. W. Cheong, "Melting of quasi-two-dimensional charge stripes in $La_{5/3}Sr_{1/3}NiO_4$," Physical Review Letters **79**, 2514–2517 (1997).

[8] P. G. Freeman, A. T. Boothroyd, D. Prabhakaran, M. Enderle, and C. Niedermayer, "Stripe order and magnetic transitions in $La_{2-x}Sr_xNiO_4$," Physical Review B **70**, 024413 (2004).

[9] S. H. Lee, S. W. Cheong, K. Yamada, and C. F. Majkrzak, "Charge and canted spin order in $La_{2-x}Sr_xNiO_4$ ($x = 0.275$ and 1/3)," Physical Review B **63**, 060405 (2001).

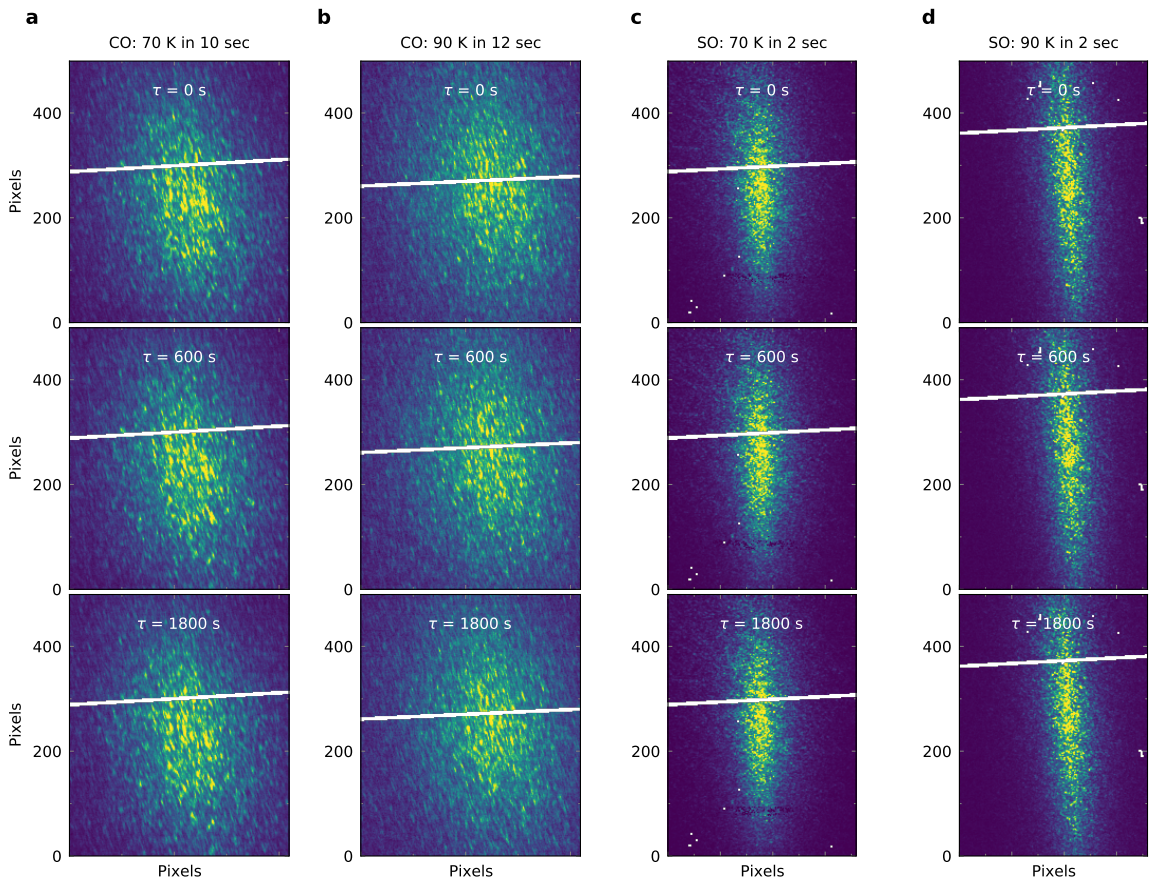

FIG. S3. Speckle patterns after different delay times at different temperatures for CO and SO.